

Carbon-oxygen ultra-massive white dwarfs in general relativity [★]

Leandro G. Althaus^{1,2,†}, Alejandro H. Córscico^{1,2}, María E. Camisassa³, Santiago Torres^{3,4},
Pilar Gil-Pons^{3,4}, Alberto Rebassa-Mansergas^{3,4} and Roberto Raddi³

¹ *Facultad de Ciencias Astronómicas y Geofísicas, Universidad Nacional de La Plata, Paseo del Bosque s/n, 1900 La Plata, Argentina*

² *Instituto de Astrofísica La Plata, UNLP-CONICET, Paseo del Bosque s/n, 1900 La Plata, Argentina*

³ *Departament de Física, Universitat Politècnica de Catalunya, c/Esteve Terrades 5, 08860 Castelldefels, Spain*

⁴ *Institute for Space Studies of Catalonia, c/Gran Capita 2–4, Edif. Nexus 104, 08034 Barcelona, Spain*

Accepted XXX. Received YYY; in original form ZZZ

ABSTRACT

We employ the La Plata stellar evolution code, LPCODE, to compute the first set of constant rest-mass carbon-oxygen ultra-massive white dwarf evolutionary sequences for masses higher than $1.29 M_{\odot}$ that fully take into account the effects of general relativity on their structural and evolutionary properties. In addition, we employ the LP-PUL pulsation code to compute adiabatic g -mode Newtonian pulsations on our fully relativistic equilibrium white dwarf models. We find that carbon-oxygen white dwarfs more massive than $1.382 M_{\odot}$ become gravitationally unstable with respect to general relativity effects, being this limit higher than the $1.369 M_{\odot}$ we found for oxygen-neon white dwarfs. As the stellar mass approaches the limiting mass value, the stellar radius becomes substantially smaller compared with the Newtonian models. Also, the thermo-mechanical and evolutionary properties of the most massive white dwarfs are strongly affected by general relativity effects. We also provide magnitudes for our cooling sequences in different passbands. Finally, we explore for the first time the pulsational properties of relativistic ultra-massive white dwarfs and find that the period spacings and oscillation kinetic energies are strongly affected in the case of most massive white dwarfs. We conclude that the general relativity effects should be taken into account for an accurate assessment of the structural, evolutionary, and pulsational properties of white dwarfs with masses above $\sim 1.30 M_{\odot}$.

Key words: stars: evolution – stars: interior – stars: white dwarfs

1 INTRODUCTION

Ultra-massive white dwarf (UMWD) stars, defined as those white dwarfs with masses higher than $\approx 1.05 M_{\odot}$, are involved in a variety of extreme astrophysical phenomena such as type Ia supernovae, micrometeorite explosions, radio transients via an accretion-induced collapse of the white dwarf (Moriya 2019), and the formation of millisecond pulsars (Wang et al. 2022), as well as stellar mergers (Cheng et al. 2020). They are also key objects for the study of the theory of high-density plasmas, general relativity, and to constrain the emission of axions (Dessert et al. 2022). Among the UMWDs, those in the highest mass range ($\gtrsim 1.30 M_{\odot}$) are crucial to constrain the initial mass threshold for the formation of white dwarfs and the electron-capture or core-collapse supernovae (Doherty et al. 2017).

The existence of UMWDs has been reported in several studies (Mukadam et al. 2004; Nitta et al. 2016; Gianninas et al. 2011; Kleinman et al. 2013; Bours et al. 2015; Kepler et al. 2016; Curd et al. 2017; Kilic et al. 2021; Hollands et al. 2020; Caiazzo et al. 2021; Jiménez-Esteban et al. 2023). In particular, the number of UMWDs with mass determinations beyond about $1.30 M_{\odot}$ has substantially increased in recent years. For instance, Gagné et al. (2018) derived a mass of $1.28 \pm 0.08 M_{\odot}$ for the

long-known white dwarf GD 50. Pshirkov et al. (2020) discovered a rapidly rotating UMWD, WDJ183202.83+085636.24, with $M = 1.33 \pm 0.01 M_{\odot}$; meanwhile, Caiazzo et al. (2021) reported the existence of a highly magnetised, rapidly rotating UMWD, ZTF J190132.9+145808.7, with a mass of $\sim 1.327\text{--}1.365 M_{\odot}$. Kilic et al. (2021) concluded that other 22 white dwarfs in the solar neighbourhood could also have masses over $1.29 M_{\odot}$, if they had pure H envelopes and CO cores.

White dwarfs with H-rich atmospheres, that is DA spectral type, and effective temperatures in the range $10\,500 \lesssim T_{\text{eff}} \lesssim 13\,000$ K exhibit pulsations due to spheroidal non-radial gravity(g) modes (Winget & Kepler 2008; Fontaine & Brassard 2008; Althaus et al. 2010; Córscico et al. 2019). These pulsating stars are called ZZ Ceti or DAV white dwarfs and constitute the most populated class of pulsating white dwarfs. Although the vast majority of ZZ Ceti stars have stellar masses in the range $0.5 \lesssim M_{\star}/M_{\odot} \lesssim 0.8$, pulsations have also been detected in, at least, four ultra-massive ZZ Ceti stars. They are BPM 37093 ($M_{\star} = 1.1 M_{\odot}$, Kanaan et al. 1992), GD 518 ($M_{\star} = 1.24 M_{\odot}$, Hermes et al. 2013), SDSS J084021 ($M_{\star} = 1.16 M_{\odot}$, Curd et al. 2017), and WD J212402 ($M_{\star} = 1.16 M_{\odot}$, Rowan et al. 2019). Recently, Kilic et al. (2023) have reported the discovery of the fifth known ultra-massive ZZ Ceti star, the DAV star WD J004917.14–252556.81, which, with M_{\star} between $\sim 1.25 M_{\odot}$ (for an ONe core) and $\sim 1.30 M_{\odot}$ (for a CO core) is the most massive pulsating white dwarf currently known. It is likely that pulsating white dwarfs as massive as WD J004917.14–252556.81 or

[★] The cooling sequences are publicly available at <http://evolgroup.fcaglp.unlp.edu.ar/TRACKS/tracks.html>

[†] E-mail: althaus@fcaglp.unlp.edu.ar

even more massive will be identified in the coming years with the advent of huge volumes of high-quality photometric data collected by space missions such as the ongoing *TESS* mission (Ricker et al. 2014) and the future *PLATO* space telescope (Rauer et al. 2014).

The increasing number of UMWDs with masses beyond $\sim 1.30 M_{\odot}$, as well as the immediate prospect of detecting pulsating white dwarfs with such masses, demand new appropriate theoretical evolutionary models to analyse them. Such new models must revise existing progenitor formation scenarios and white dwarf evolution, and contemplate the introduction of more realistic input physics. In particular, it is necessary to calculate models that take into account general relativity effects and to evaluate the resulting pulsational properties.

Theoretical evolutionary scenarios predict an oxygen-neon (ONe) or carbon-oxygen (CO) core-chemical composition for UMWDs. ONe core white dwarfs are expected to result from the semi-degenerate carbon burning during the single evolution of massive intermediate-mass stars that evolve to the super asymptotic giant branch. The initial mass threshold for carbon burning is around $6-9 M_{\odot}$, and was reported to depend mainly on the metallicity and the treatment of convective boundaries (García-Berro et al. 1997; Gil-Pons et al. 2005; Siess 2006; Ventura & D’Antona 2011; Doherty et al. 2015). The effects of rotation and nuclear reaction rates are also known to affect this mass threshold (Doherty et al. 2017). The formation of an ONe core composition in UMWDs is also predicted by the merger of two white dwarfs as a result of off-center carbon burning in the merged remnant when the remnant mass is larger than $1.05 M_{\odot}$ (Schwab 2021a).

On the other hand, CO UMWDs can result from single stellar evolution (see Althaus et al. 2021). In particular, these authors have shown that isolated progenitors of UMWDs can avoid C burning on the asymptotic giant branch, supporting the existence of CO cores in white dwarfs more massive than $1.05 M_{\odot}$. Specifically, reduced wind rates with respect to the standard prescriptions and/or the occurrence of core rotation (which lowers the internal pressure, see also Dominguez et al. 1996) hamper C-ignition, thus favouring the formation of UMWDs with CO cores. In addition, the formation of UMWDs with CO cores can also result from white dwarf merger, see Wu et al. (2022). These authors have shown that CO UMWDs with masses below $1.20 M_{\odot}$ can be produced from massive CO white dwarfs + He white dwarf merger. The merger scenario for the formation of UMWDs is sustained by the fact that a considerable fraction of the massive white dwarf population is thought to be formed as a result of stellar mergers (Temminck et al. 2020; Cheng et al. 2020; Torres et al. 2022).

The study of the evolution of UMWDs has been the subject of numerous recent papers. In particular, Camisassa et al. (2019) studied in detail the full evolution of ONe UMWDs with masses up to $1.29 M_{\odot}$ considering realistic initial chemical profiles that are the result of the full progenitor evolution calculated in Siess (2010). More recently, Althaus et al. (2021) and Camisassa et al. (2022) computed the evolution of UMWDs up to $1.29 M_{\odot}$ with CO cores resulting from the complete evolution of single progenitor stars that avoid the C-ignition during the super asymptotic giant branch (see Althaus et al. 2021). Finally, Schwab (2021b) studied the evolution of white dwarfs more massive than $1.29 M_{\odot}$, with the focus on neutrino cooling via the Urca process, showing that this process is important for the age determination of ONe core white dwarf stars.

For the most massive white dwarfs, the importance of general relativity for their structure and evolution cannot be completely disregarded. In fact, numerous works based on static white dwarf structures have shown that general relativistic effects are relevant for the

determination of the radius of massive white dwarfs (Rotondo et al. 2011; Mathew & Nandy 2017; Carvalho et al. 2018; Nunes et al. 2021). In particular, these studies demonstrated that for fixed values of mass, deviations up to 50% in the Newtonian white dwarf radius are expected compared to the general relativistic white dwarf radius. More recently, Althaus et al. (2022) have presented the first set of constant rest-mass ONe UMWD evolutionary models more massive than $1.30 M_{\odot}$ that fully take into account the effects of general relativity. This study demonstrates that the general relativity effects must be taken into account to assess the structural and evolutionary properties of the most massive white dwarfs.

In this paper, we extend the relativistic calculations presented in Althaus et al. (2022) to the case of UMWDs with CO cores that result from the complete evolution of single progenitor stars that avoid C-ignition (see Althaus et al. 2021). We employ the La Plata stellar evolution code, LPCODE, to compute full evolutionary sequences of white dwarfs more massive than $1.29 M_{\odot}$, taking into account general relativity effects. For comparison purposes, additional sequences of identical initial models are computed for the Newtonian gravity case. We also employ the LP-PUL pulsation code to perform an exploratory pulsational investigation by computing g -mode Newtonian pulsations on fully relativistic equilibrium white dwarf models and comparing the results of the period spacings and oscillation kinetic energies with the case of Newtonian white dwarf models. The strong effects of general relativity on the thermo-mechanical structure of the most massive CO white dwarfs we report in this work may impact the energetics of the explosion and the nucleosynthesis of neutron-rich matter, and thus be relevant for the better understanding of type-Ia supernova explosions. Furthermore, general relativity effects could affect the critical density that separates the explosive and the collapse outcomes of these supernovae (Bravo & García-Senz 1999).

This paper is organised as follows. In Sect. 2 we provide the main computational details and input physics of our relativistic white dwarf sequences. Sect. 3 is devoted to explore the impact of general relativity effects on the relevant evolutionary properties of our massive white dwarfs. In this section we also compare the predictions of our new white dwarf sequences with observational data of UMWDs. In Sect. 4 we assess the Newtonian pulsational properties of relativistic white dwarf models, and compare them with the pulsational properties of Newtonian models. Finally, in Sect. 5 we summarise the main findings of this work.

2 COMPUTATIONAL DETAILS AND INPUT PHYSICS

The set of CO UMWD evolutionary sequences was computed with the stellar evolution code LPCODE, developed by the La Plata group (Althaus et al. 2005; Salaris et al. 2013; Althaus et al. 2015; Miller Bertolami 2016; Silva Aguirre et al. 2020; Christensen-Dalsgaard et al. 2020). It has been modified to include the effects of general relativity, following the formalism given in Thorne (1977), see Althaus et al. (2022) for details about the implementation of pertinent general relativity equations in LPCODE. In particular, the fully general relativistic partial differential equations governing the evolution of a spherically symmetric star are formulated in a way that they resemble the standard Newtonian equations of stellar structure and evolution. Of relevance in this formulation are the dimensionless general relativistic correction factors that are applied on these equations, that is \mathcal{H} , \mathcal{E} , \mathcal{V} , and \mathcal{R} , which correspond to the enthalpy, gravitational acceleration, volume, and redshift correction factors, respectively. These factors turn to unity in the Newtonian limit, and are given by the expressions:

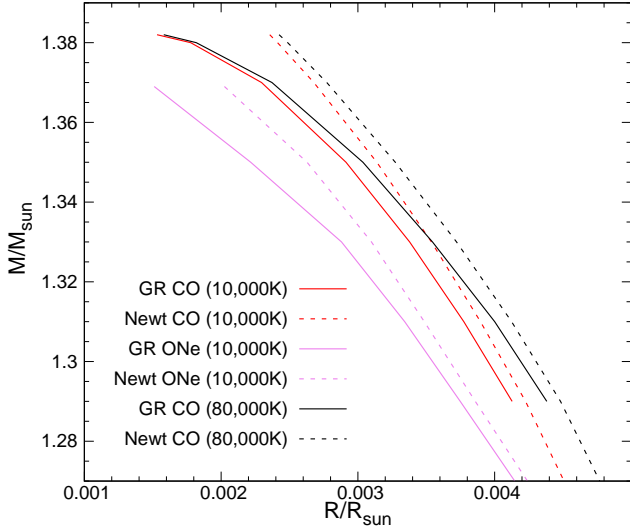


Figure 1. Gravitational mass versus stellar radius for our CO UMWD models considering and disregarding the effects of general relativity (solid and dashed lines, respectively). Models are shown at $T_{\text{eff}} = 10\,000$ and $80\,000$ K (red and black lines, respectively). In addition, the mass-radius relations for ONe white dwarfs at $T_{\text{eff}} = 10\,000$ K taken from [Althaus et al. \(2022\)](#) are shown with violet lines.

$$\mathcal{H} = \frac{\varrho^t}{\varrho} + \frac{P}{\varrho c^2}, \quad (1)$$

$$\mathcal{E} = \frac{m^t + 4\pi r^3 P/c^2}{m}, \quad (2)$$

$$\mathcal{V} = \left(1 - \frac{2Gm^t}{rc^2}\right)^{-1/2}, \quad (3)$$

$$\mathcal{R} = e^{\Phi/c^2}, \quad (4)$$

where m is the rest mass inside a radius r or baryonic mass, ϱ is the density of rest mass, m^t is the mass-energy inside r and includes contributions from the rest-mass energy, the internal energy, and the gravitational potential energy, which is negative. Since the internal and gravitational potential energy change during the course of evolution, the stellar mass-energy is not a conserved quantity. ϱ^t is the density of the total non-gravitational mass-energy, and includes the density of the rest mass plus contributions from the kinetic and potential energy densities due to particle interactions (it does not include the gravitational potential energy density), that is, $\varrho^t = \varrho + (u\varrho)/c^2$, where u is the internal energy per unit mass. Φ is the general relativistic gravitational potential related to the temporal metric coefficient.

The rest of adopted input physics for our relativistic CO white dwarf models is the same as that in [Camisassa et al. \(2022\)](#), except that in the present work we did not explore the impact of ^{22}Ne sedimentation on the cooling of white dwarfs. We omitted the energy generation by nuclear reactions since these are not happening in our white dwarf models. We also disregarded neutrino cooling via the Urca process, despite the fact that they are not entirely negligible in CO UMWDs, see [Schwab \(2021b\)](#). Hence, the cooling times of our relativistic sequences may be somewhat overestimated at high and intermediate luminosities. The energetics resulting from crystallization processes in the core was included as in [Camisassa et al. \(2022\)](#), and takes into account the release of latent heat and the heat resulting from phase separation of carbon and oxygen during crystallization.

We computed the full evolution of constant rest-mass CO UMWDs

with masses of 1.29, 1.31, 1.33, 1.35, 1.37, 1.38, and $1.382 M_{\odot}$. Here, the white dwarf mass means the total rest mass or baryonic mass of the white dwarf, which remains constant throughout the cooling process. This mass should not be confused with the total gravitational mass, M_G (the value of m^t at the surface of the star), that is, the stellar mass that would be measured by a distant observer. M_G changes during the course of white dwarf evolution and turns out to be slightly lower than the total baryonic mass of the white dwarf, see [Table 1](#). As shown in [Althaus et al. \(2021\)](#), CO UMWDs can result from single stellar evolution if C burning on the asymptotic giant branch is avoided. In particular, for all the white dwarf models we employed the chemical profile of the $1.159 M_{\odot}$ CO-core hydrogen-rich white dwarf resulting from the complete evolution of an initially $7.8 M_{\odot}$ model that avoids C-ignition, and whose CO core slowly grows during the super asymptotic giant branch as a result of reduced wind rates (see [Althaus et al. 2021](#)). This progenitor evolution was computed with the Monash-Mount Stromlo code as presented in [Gil-Pons et al. \(2013, 2018\)](#). The set of relativistic cooling sequences of CO UMWDs presented in this work extends the mass range of the CO white dwarf sequences already computed in [Camisassa et al. \(2022\)](#) within the framework of the Newtonian theory of stellar interiors.

3 IMPACT OF GENERAL RELATIVITY ON THE EVOLUTION OF MASSIVE CO WHITE DWARFS

We describe now the main consequences of general relativity on the properties of CO UMWDs. In [Fig. 1](#) we show the resulting mass-radius relation at two different effective temperatures. Specifically, the gravitational mass is depicted in terms of the stellar radius for our CO UMWD models considering and disregarding the effects of general relativity (solid and dashed lines, respectively) at $T_{\text{eff}} = 10\,000$ and $80\,000$ K, red and black lines, respectively. We mention that the gravitational mass is lower by 0.02% than the baryonic stellar mass, see [Table 1](#). At a given mass, the stellar radius is smaller in the case that general relativity effects are taken into account, particularly for highest stellar masses where general relativity plays a major role. In both cases, the impact of finite temperature on the stellar radius is noticeable only at lower stellar masses and appears to show a somewhat higher variation with the stellar mass when the general relativity effects are introduced. For comparison purposes, we also show in [Fig. 1](#) the mass-radius relations for ONe white dwarfs at $T_{\text{eff}} = 10\,000$ K taken from [Althaus et al. \(2022\)](#) (violet lines). Because of the stronger Coulomb interaction in ONe cores, the stellar radius results smaller in ONe-core white dwarfs than in CO-core ones with the same mass.

In our calculations, CO white dwarfs more massive than $1.382 M_{\odot}$ become gravitationally unstable with respect to general relativity effects, being this limit higher than the $1.369 M_{\odot}$ we found for ONe white dwarfs, [Althaus et al. \(2022\)](#). This happens at a given finite central density somewhat larger than $2 \times 10^{10} \text{ g cm}^{-3}$ (see [Table 1](#)). This limiting mass is in agreement with the findings of zero-temperature predictions by [Rotondo et al. \(2011\)](#) for pure-oxygen and pure-carbon white dwarfs (1.380 and $1.386 M_{\odot}$, respectively) and with [Mathew & Nandy \(2017\)](#) for white dwarfs composed of oxygen ($1.385 M_{\odot}$) and carbon ($1.391 M_{\odot}$). We note that the central density of our $1.382 M_{\odot}$ white dwarf model in the general relativity case is near the density threshold for inverse β -decays for oxygen composition, $1.90 \times 10^{10} \text{ g cm}^{-3}$, see [Mathew & Nandy \(2017\)](#). For carbon composition, the corresponding threshold density is $3.9 \times 10^{10} \text{ g cm}^{-3}$, so the central density is limited by general relativity rather

Table 1. Relevant characteristics of our sequences at $T_{\text{eff}} = 10\,000\text{ K}$. M_{WD} : total baryonic mass. M_{G} : total gravitational mass. R^{Newt} : stellar radius in the Newtonian case. R^{GR} : stellar radius in the general relativity case. g^{Newt} : surface gravity in the Newtonian case. g^{GR} : surface gravity in the general relativity case. ρ_c^{Newt} : central density in the Newtonian case. ρ_c^{GR} : central density of rest mass in the general relativity case.

M_{WD} M_{\odot}	M_{G} M_{\odot}	R^{Newt} R_{\odot}	R^{GR} R_{\odot}	$\log g^{\text{Newt}}$ cm s^{-2}	$\log g^{\text{GR}}$ cm s^{-2}	ρ_c^{Newt} g cm^{-3}	ρ_c^{GR} g cm^{-3}
1.29	1.28978	0.00422592	0.00412784	9.296	9.317	4.88×10^8	5.34×10^8
1.31	1.30977	0.00389625	0.00377446	9.374	9.402	6.74×10^8	7.61×10^8
1.33	1.32975	0.00353773	0.00337825	9.464	9.505	9.84×10^8	1.17×10^9
1.35	1.34974	0.00313854	0.00291305	9.574	9.640	1.56×10^9	2.05×10^9
1.37	1.36972	0.00267802	0.00229552	9.719	9.854	2.82×10^9	4.91×10^9
1.38	1.37971	0.00241236	0.00177701	9.813	10.079	4.13×10^9	1.21×10^{10}
1.382	1.38170	0.00235540	0.00153125	9.834	10.210	4.50×10^9	2.03×10^{10}

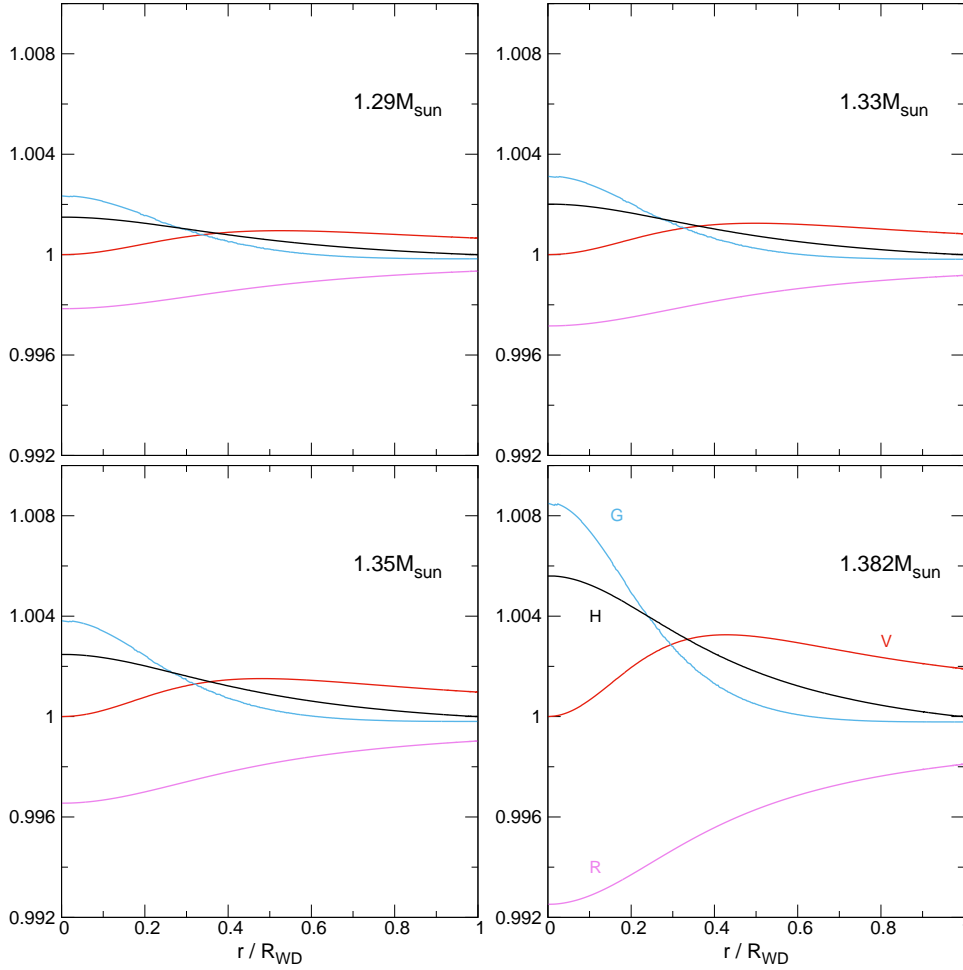


Figure 2. Run of general relativistic correction factors \mathcal{H} , \mathcal{G} , \mathcal{V} , and \mathcal{R} (black, blue, red, and violet lines, respectively) for 1.29, 1.33, 1.35, and 1.382 M_{\odot} white dwarf models at $\log L/L_{\odot} = -3$ in terms of the fractional radius. These factors turn to unity in the Newtonian limit.

than electron captures in carbon white dwarfs. Consequently, the fact that we have not considered eventual instabilities against the inverse β -decays should not affect the reliability of our models, at least up to white dwarf masses of 1.380 M_{\odot} .

The major role played by general relativity for increasing stellar masses is expected from the dependence of the general relativistic correction factors with the stellar mass, as illustrated by Fig. 2. This figure displays \mathcal{H} , \mathcal{G} , \mathcal{V} , and \mathcal{R} (black, blue, red, and violet lines, respectively) in terms of the fractional radius for the 1.29, 1.33,

1.35, and 1.382 M_{\odot} white dwarf models at $\log L/L_{\odot} = -3$. As mentioned, these factors are equal to one in the Newtonian limit, and have a slight dependence on the effective temperature. Their behaviour is related to curvature effects, as well as to the fact that the pressure and the internal energy appear as a source of gravity in general relativity, which implies that both density and pressure gradients need to be steeper than in Newtonian gravity to maintain hydrostatic equilibrium. This causes the factors \mathcal{G} and \mathcal{H} , which depend on density and pressure, to increase towards the center of

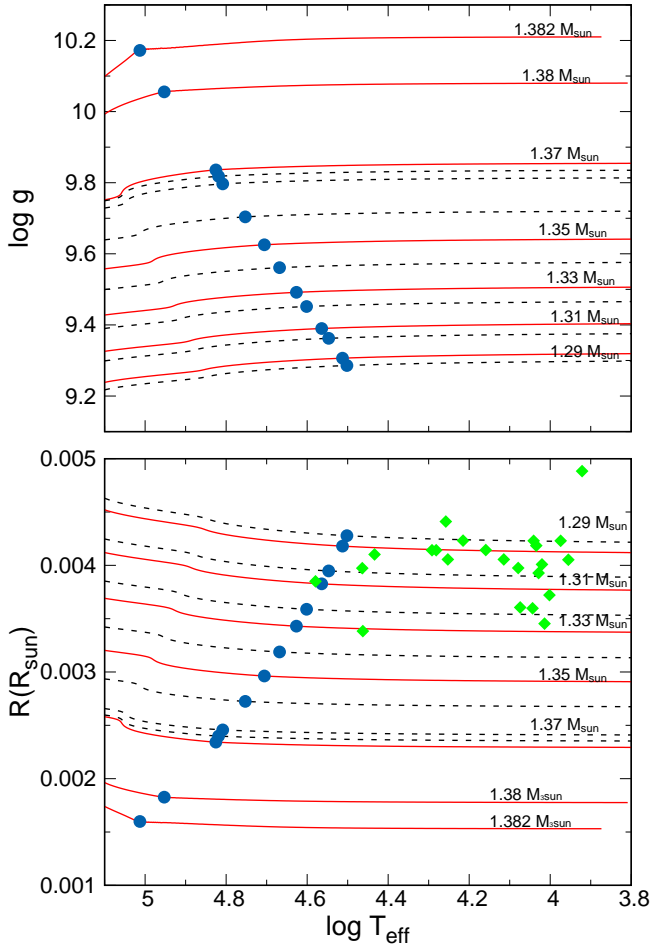


Figure 3. Surface gravity and stellar radius (in solar units) in terms of effective temperature for all of our sequences are displayed in the upper and bottom panels, respectively. Red solid and black dashed lines correspond to the general relativity and Newtonian cases, respectively. From bottom (top) to top (bottom), curves in the upper (bottom) panel correspond to 1.29, 1.31, 1.33, 1.35, 1.37, 1.38, and 1.382 M_{\odot} CO white dwarf cooling sequences. Blue filled circles denote the onset of core crystallization in each sequence. The most massive white dwarfs in the solar neighbourhood analysed in Kilic et al. (2021) are displayed using green filled diamonds.

the star. The relativistic factor \mathcal{V} , a correction to the volume, is equal to one at the center of the star where the volume is zero and attains a maximum value at some inner point in the star. Towards the surface of the star, \mathcal{G} and \mathcal{H} tend to M_G/M_{WD} and 1, respectively. We mention that the behaviour of the general relativistic correction factors depicted in Fig. 2 qualitatively resemble those exhibited by the ONe UMWDs (see Althaus et al. 2022).

In Fig. 3 we illustrate the surface gravity and the stellar radius in terms of the effective temperature for all of our sequences for the general relativity and Newtonian cases, using solid and dashed lines, respectively. The gravitational field for the general relativistic sequences corresponds to the gravitational field as measured far from the star, and is given by

$$g^{\text{GR}} = \frac{Gm}{r^2} \mathcal{G} \mathcal{V}^2. \quad (5)$$

Clearly, the surface gravity and stellar radius are markedly affected by general relativity, particularly for the most massive sequences. We

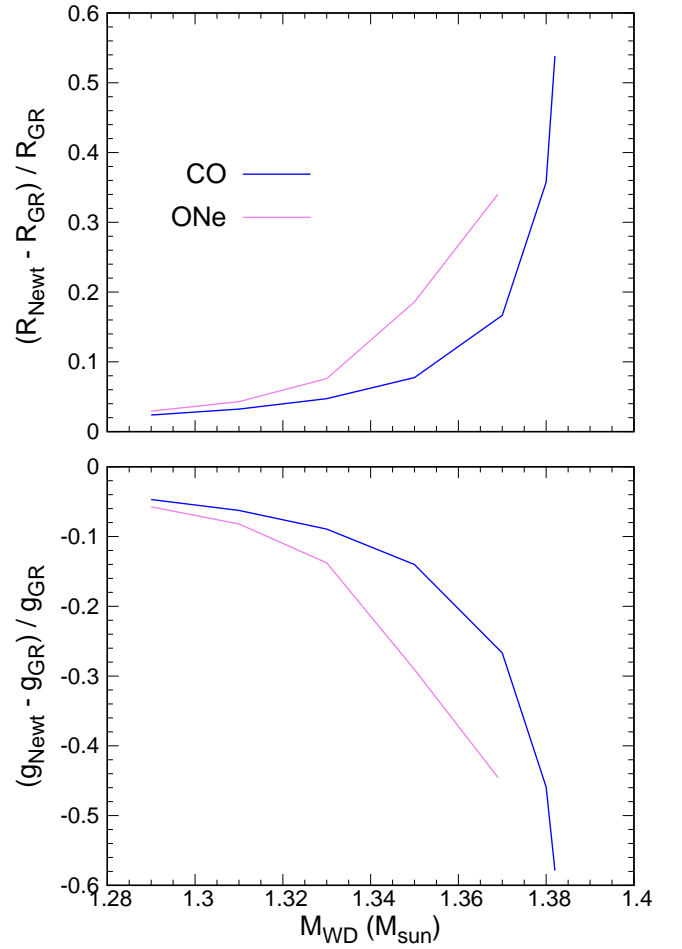


Figure 4. Upper panel: Relative difference between Newtonian stellar radius and general relativistic stellar radius in terms of the stellar mass. Results are for our CO and ONe UMWD models (blue and violet lines, respectively) at $T_{\text{eff}} = 10000$ K. Bottom panel: same as upper panel but for the surface gravity.

note that not considering the general relativity effects would yield a stellar mass value about 0.015 M_{\odot} larger for cool white dwarfs with measured surface gravities of $\log g \approx 9.8$. The photometric measurements of Kilic et al. (2021) for the radius of the UMWDs in the solar neighbourhood are also plotted in this figure. According to our CO ultra-massive relativistic sequences, the most massive white dwarfs of this sample have masses near 1.33 M_{\odot} . Such value turns out to be 1.34 M_{\odot} if Newtonian sequences were used instead.

In Fig. 4 we show the relative difference in stellar radius and gravity, upper and lower panel, respectively, between Newtonian and general relativistic predictions versus the stellar mass for our CO UMWD models at $T_{\text{eff}} = 10000$ K. For comparison purposes we also show the predictions for the relativistic ONe white dwarfs from Althaus et al. (2022) (violet lines). Clearly, differences increase markedly as the stellar mass approaches our maximum mass value, 1.382 M_{\odot} , for which the relative difference in radius (taking as a reference the relativistic model) is about 55%. The stellar radius at this stellar mass results 1070 km in the general relativity case (see Table 1), which is nearly 40% smaller than the moon radius. For stellar masses lower than $\approx 1.29 M_{\odot}$, differences in the stellar radius resulting from general relativistic corrections become lower than 2%.

The onset of core crystallization in each sequence depicted in

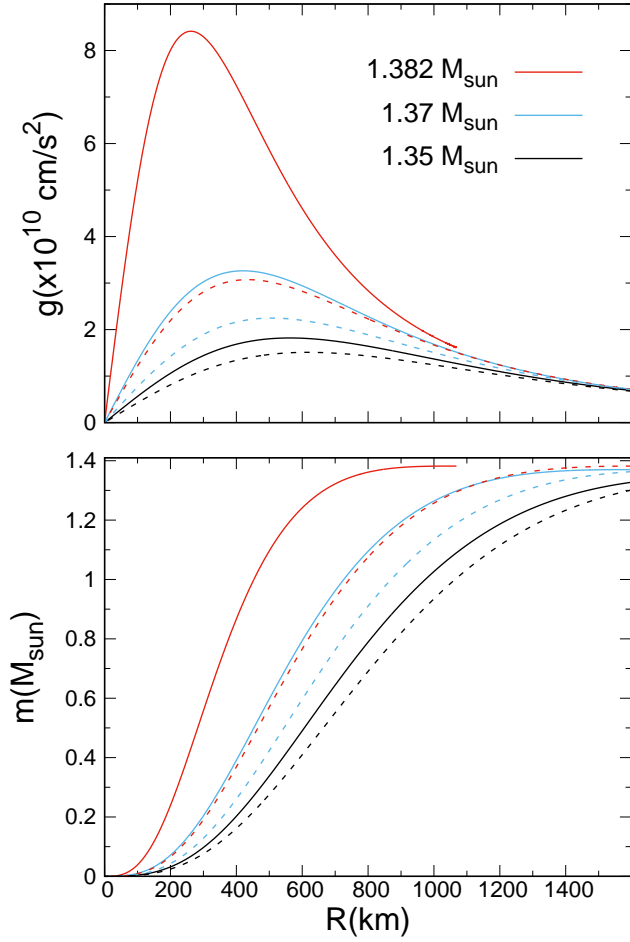


Figure 5. Gravitational field (upper) and rest mass m (bottom panel) for the general relativity and Newtonian cases (solid and dashed lines, respectively) in terms of radial coordinate for 1.382, 1.37, and $1.35 M_{\odot}$ CO white dwarf models at $T_{\text{eff}} = 11\,000 \text{ K}$ (red, blue, and black lines, respectively).

Fig. 3 is marked with blue filled circles. Because of the denser and cooler cores of the general relativistic white dwarfs (see later in this section), core crystallization at a given stellar mass begins at higher effective temperatures than in their Newtonian counterparts. This is particularly evident for the $1.382 M_{\odot}$ white dwarf sequence. We note that for this stellar mass, general relativity predicts that a 70% of the white dwarf mass has crystallised by the time the onset of core crystallization takes place in the Newtonian case. The marked reduction in the radius at high effective temperatures before the onset of crystallization is due to the dominance of neutrino cooling at those evolutionary stages.

The run of the inner gravitational field and rest mass versus radial coordinate for the 1.382, 1.37, and $1.35 M_{\odot}$ CO white dwarf models at $T_{\text{eff}} = 10\,000 \text{ K}$ is shown in Fig. 5 (upper and bottom panel, respectively) for the general relativity and Newtonian cases (solid and dashed lines, respectively). In the case of the most massive model, general relativity effects strongly impact the stellar structure. We note in particular the noticeable differences in the gravitational field, as compared with Newtonian predictions. The impact is also evident toward lower stellar masses, albeit to a lesser extent. In Fig. 6 we show the run of temperature and density of rest mass for the general relativity and Newtonian cases (solid and dashed lines, respectively)

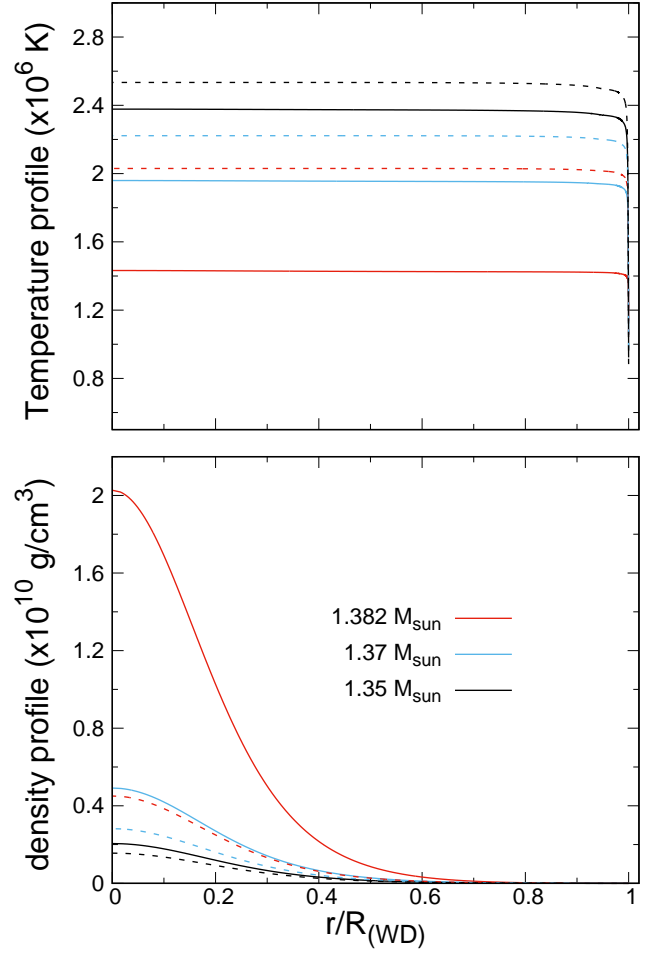


Figure 6. Temperature (upper panel) and density of rest mass (bottom panel) for the general relativity and Newtonian cases (solid and dashed lines, respectively) in terms of radial coordinate for the same CO white dwarf models as depicted in Fig. 5.

in terms of radial coordinate for the same CO white dwarf models as depicted in Fig. 5. We note the larger inner densities in the general relativity models, as compared to the Newtonian case, particularly for the most massive white dwarf model. In addition, appreciable differences arise in the internal temperature profile. Models with $1.382 M_{\odot}$ ($1.35 M_{\odot}$) computed considering general relativity have central temperatures about 30% (6%) cooler than their Newtonian counterparts during most of cooling stages.

An important observational constraint to the mass-radius relation of white dwarfs is provided by the measurement of the gravitational redshift, related to the fact that photons lose energy when escaping from the surface of a white dwarf. The resulting change in the photon wavelength (λ) is related to the recession velocity by, see Chandra et al. (2020):

$$v_g = c \frac{\Delta\lambda}{\lambda}, \quad (6)$$

where

$$\frac{\Delta\lambda}{\lambda} = \mathcal{Z} - 1. \quad (7)$$

Here, \mathcal{Z} is given by assessing Eq. 3 at the stellar surface. Since

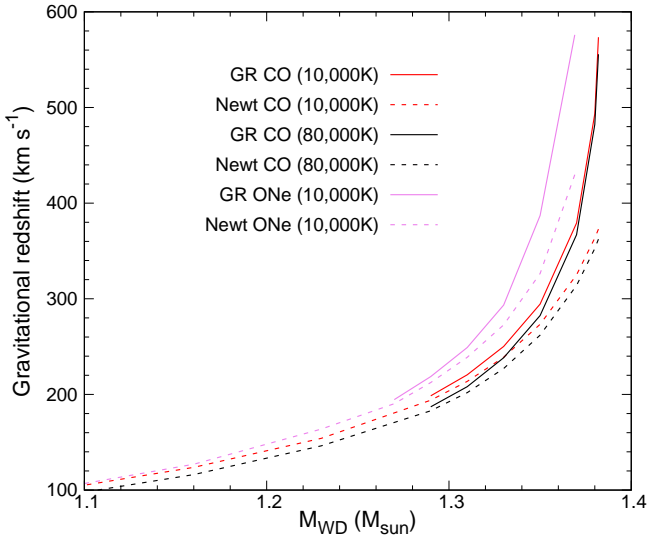


Figure 7. Gravitational redshift versus stellar mass for our CO UMWD models considering and disregarding the effects of general relativity (solid and dashed lines, respectively). Models are shown at $T_{\text{eff}} = 10\,000$ and $80\,000$ K (red and black lines, respectively). In addition, the gravitational redshift for ONe white dwarfs at $T_{\text{eff}} = 10\,000$ K is shown with violet lines.

the gravitational redshift depends directly on the mass and radius of the white dwarf, we expect this quantity to be altered by general relativity in massive white dwarfs. This is borne out by Fig. 7, which depicts the gravitational redshift in terms of the stellar mass for our CO UMWD models considering and disregarding the effects of general relativity (solid and dashed lines, respectively) at $T_{\text{eff}} = 10\,000$ and $80\,000$ K (red and black lines, respectively). For comparison purposes, predictions for ONe white dwarfs from Althaus et al. (2022) at $T_{\text{eff}} = 10\,000$ K are also shown. For the most massive white dwarf models, the inclusion of general relativity effects leads to a gravitational redshift a factor 1.5 larger than predicted by the Newtonian white dwarf models (differences in the gravitational redshift are about 200 km s^{-1}). This result was expected since v_g varies essentially as $\approx M/R$, and the stellar radius is markedly smaller when general relativity is taken into account. For masses below $1.29 M_{\odot}$, differences in the gravitational redshift are below $2\text{--}3\text{ km s}^{-1}$. Because ONe white dwarfs are more compact than CO ones, a larger gravitational redshift is expected in these stars.

In Fig. 8 we illustrate the cooling times of our CO UMWDs for the general relativity and Newtonian cases, with solid and dashed lines, respectively. The cooling times are set to zero at the beginning of the cooling tracks at very high effective temperatures. As in the case of ONe white dwarfs we studied in Althaus et al. (2022), the cooling behaviour is substantially altered by general relativity effects. In the case of the most massive white dwarf, general relativity causes CO UMWDs to evolve faster than in the Newtonian case at advanced stages of evolution. In particular, the $1.382 M_{\odot}$ relativistic sequence requires half the time to reach the low luminosity stages than needed in the Newtonian case. The trend in the cooling behaviour is reversed at earlier stages of evolution, where white dwarfs computed in the general relativity case evolve more slowly than their Newtonian counterparts, see Althaus et al. (2022) for a similar behaviour and explanation.

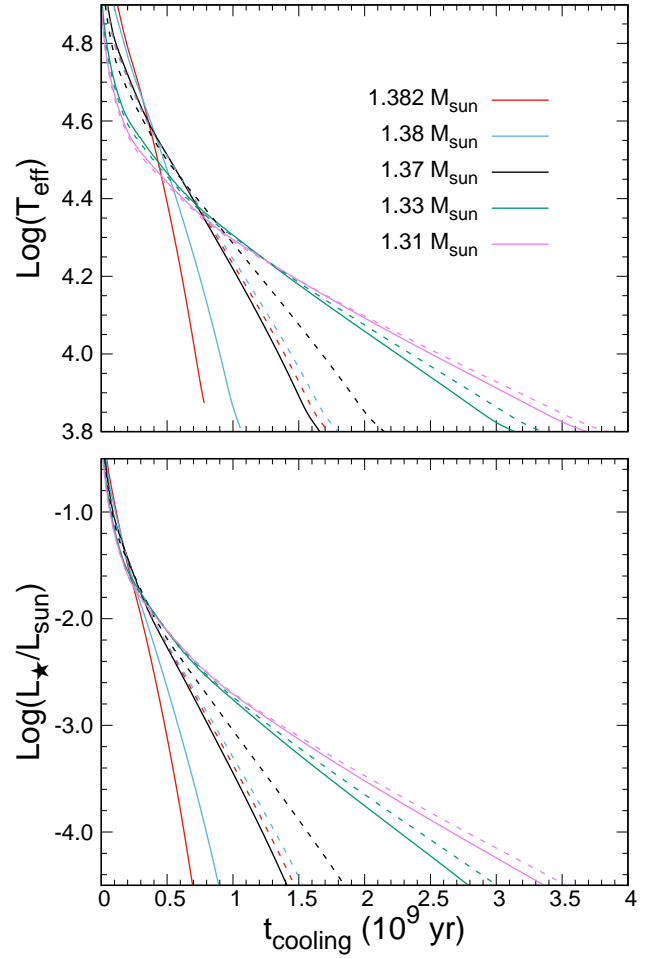


Figure 8. Effective temperature and surface luminosity (upper and bottom panels) versus the cooling times for our 1.31 , 1.33 , 1.37 , 1.38 , and $1.382 M_{\odot}$ CO white dwarf sequences. Solid (dashed) lines correspond to the general relativity (Newtonian) cases. Cooling time is counted from the time of white dwarf formation.

3.1 Relativistic UMWD *Gaia* candidates

The *Gaia* mission has provided an unprecedented increase in both the quality and the number of known white dwarfs in our solar neighbourhood. Recently, Torres et al. (2023; submitted) analysed a sample of nearly 90 000 white dwarfs within 500 pc from the Sun obtained from *Gaia* DR3 data. The sample has been selected applying the same criteria as in (Jiménez-Esteban et al. 2023) but extended up to 500 pc. Although completeness is not guaranteed, the applied selection criteria ensure good quality data (i.e., photometric and astrometric errors below 10%). In Fig. 9 we show the *Gaia* Hertzsprung-Russell diagram for the entire sample (red dots) of the white dwarf population. Superimposed are the *Gaia* magnitudes¹ tracks for our relativistic and Newtonian CO cooling sequences (solid black and dashed blue lines, respectively). Isochrones of 0.25, 0.5, 1, and 2 Gyr for our relativistic sequences are also shown with dotted black lines. An inspection of the *Gaia* colour-magnitude diagram reveals an important set of objects with masses higher than $1.29 M_{\odot}$ (red filled circles)

¹ Sloan Digital Sky Survey, Pan-STARRS and other passbands are also available upon request using the non-grey model atmospheres of Koester (2010) and Koester & Kepler (2019).

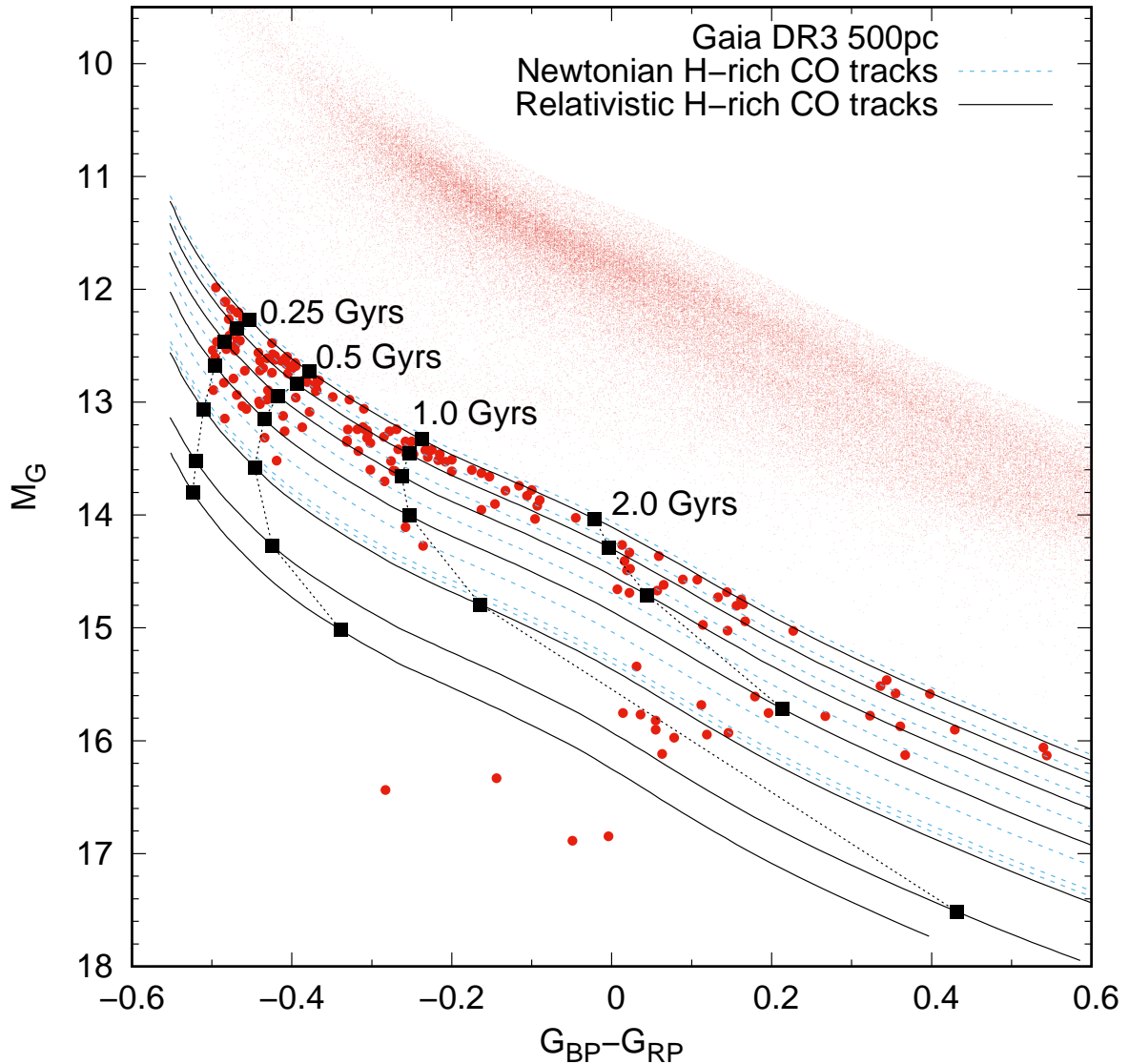


Figure 9. *Gaia* colour-magnitude diagram. Newtonian and general relativistic CO-core cooling sequences are displayed using dashed blue and solid black lines, respectively. Their rest masses are, from top to bottom, 1.29, 1.31, 1.33, 1.35, 1.37, 1.38 and 1.382 M_{\odot} . The *Gaia* DR3 white dwarf population within 500 pc from Torres et al. (2023; submitted), is displayed using red dots. Among these objects, we highlighted the UMWDs located below the 1.29 M_{\odot} cooling track using red filled circles. Dotted black lines display isochrones of 0.25, 0.5, 1, and 2 Gyrs.

that can be considered as reliable UMWD candidates. Among these candidates we clearly identify those belonging to the so-called faint-blue branch ($M_G > 15$) that deserve a separate analysis (see for instance Scholz 2022; Althaus et al. 2022; Bergeron et al. 2022). For the rest of objects, around 25 of them lay in the colour-magnitude region corresponding to masses larger than 1.33 M_{\odot} . It is beyond the purpose of the present work to fully analyse these objects, as it would require higher accurate observations; however, they can be presented as reasonable UMWD candidates of our solar neighbourhood for which general relativistic effects should be taken into account. In the case of the most massive white dwarfs, general relativity effects lead to white dwarf sequences that are markedly fainter than Newtonian sequences with the same mass. Thus, the effects of general relativity must be carefully taken into account when determining the mass and stellar properties of such massive white dwarfs through *Gaia* photometry. Not considering such effects would lead to an over-

estimation of their mass and an incorrect estimation of their cooling times.

4 PULSATONAL PROPERTIES OF RELATIVISTIC WHITE DWARF MODELS

Given the continuous arrival of large amounts of photometric data of pulsating white dwarfs from space missions such as the ended *Kepler/K2* program and the ongoing *TESS* mission, we believe to be worthwhile to assess the pulsational properties of our relativistic UMWDs. As a first step, we limit ourselves to calculate Newtonian pulsations of non-radial g modes on fully relativistic CO UMWD models, similar to what was done in the preliminary calculations of Córscico et al. (2023) for ONe UMWDs. The assessment of the combined effects of considering relativistic ONe- and CO-core UMWD models *along with* fully relativistic g -mode pulsations, will be the focus of a future publication (Córscico et al. 2023, in preparation).

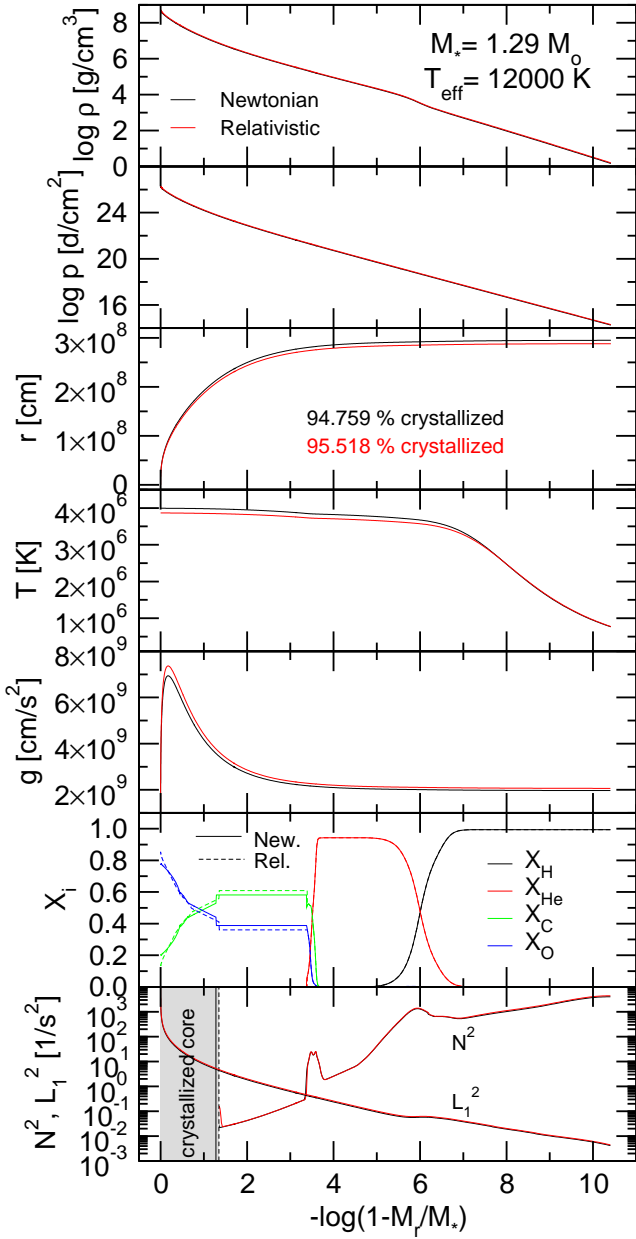


Figure 10. Newtonian (black curves) and relativistic (red curves) properties of a template UMWD model characterised by $M_\star = 1.29 M_\odot$ and $T_{\text{eff}} \sim 12000$ K. From top to bottom, we depict the run of the logarithm of the density (ρ), the logarithm of pressure (p), the radius r , the temperature (T), the gravity (g), the internal chemical profiles (X_i), and the squared critical Brunt-Väisälä and Lamb ($\ell = 1$) frequencies, in terms of the outer mass fraction coordinate. The grey region in the bottom panel represents the crystallised core, in which the g mode-pulsations are inhibited. In the plot of the chemical profiles and location of the crystallization front, solid (dashed) curves correspond to the Newtonian (relativistic) case.

We have selected two pairs of template CO white dwarf models with $M_\star = 1.29 M_\odot$ and $M_\star = 1.382 M_\odot$, each couple of models considering and disregarding the effects of general relativity. These models have $T_{\text{eff}} = 12000$ K, an effective temperature representative of the instability strip of the ZZ Ceti variables. We have computed non-radial g modes with periods between 50 s and 1500 s for these template models using an adiabatic version of the LP-PUL pulsation code (Córscico & Althaus 2006) that assumes the "hard-sphere"

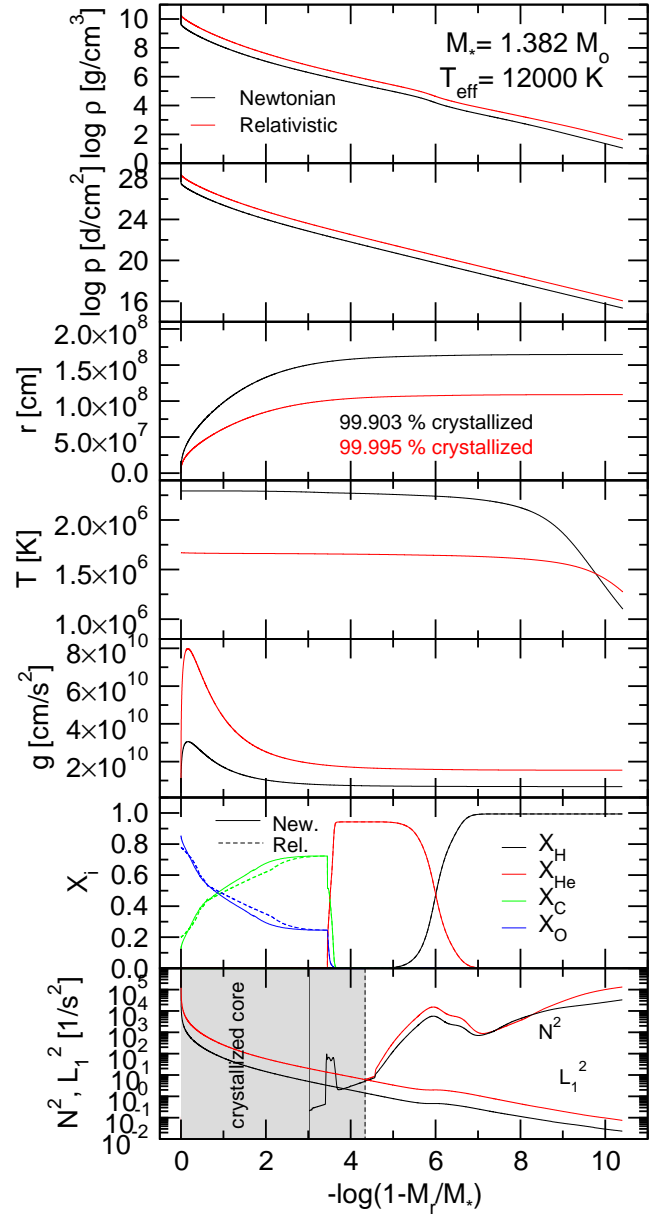


Figure 11. Same as in Fig. 10, but for the case of a UMWD model with $M_\star = 1.382 M_\odot$.

boundary conditions for the eigenfunctions at the edge of the solid core of crystallizing white dwarf models (Montgomery & Winget 1999). We show in Fig. 10 the logarithm of the density, pressure, the stellar radius, the temperature, the gravity, the internal chemical profiles, and the squared Brunt-Väisälä and Lamb ($\ell = 1$) frequencies, in terms of logarithm of the outer mass fraction coordinate, corresponding to the template UMWD model characterised by $M_\star = 1.29 M_\odot$ and $T_{\text{eff}} \sim 12000$ K. Black curves correspond to the Newtonian case, while red curves are display the fully relativistic case. Clearly, general relativity induces smaller radii and temperatures, and larger gravities, as compared with the Newtonian case. The effect on the density and pressure profiles is hardly visible, but non negligible. Also, no appreciable differences arise in the crystallised mass from the two models. Finally, the effect of considering Newtonian or relativistic gravitation has very little impact on the chemical composition profiles and on the Brunt-Väisälä and Lamb frequencies.

The situation is completely different when we consider more massive models, as can be seen in Fig. 11, that show the same quantities as in Fig. 10, but for the case of the template models with $M_{\star} = 1.382 M_{\odot}$. As we described previously, in this case, there is a very large variation in the stellar radius, gravity and temperature when relativistic effects are taken into account. The change in density and pressure is now noticeable (note that these quantities are plotted on a logarithmic scale). The strong impact of considering relativistic or Newtonian gravity is reflected in major differences in the Brunt Väisälä and Lamb frequency profiles (see the lower panels of Fig. 11). In addition, we note that in the relativistic model, the CO/He interface is reached by the crystallization front, in contrast with the situation for the Newtonian model.

The impact on the pulsational properties of considering fully relativistic UMWD models in comparison with models assuming Newtonian gravity is shown in Fig. 12 for the two values of stellar mass considered. The figure displays the forward period spacing (upper panels) and the kinetic energy of oscillation of modes (lower panels), in terms of the dipole g -mode periods. Not surprisingly, adopting general relativity does not have a significant impact neither on the period spacing nor on the kinetic energy of the modes for the case of the models with $M_{\star} = 1.29 M_{\odot}$ (left panels). In contrast, there is a significant impact in the $1.382 M_{\odot}$ model (right panels). Indeed, the asymptotic period spacing (dashed horizontal lines) for the relativistic case is about five seconds shorter than for the Newtonian model. This is because the Brunt-Väisälä frequency is higher for the relativistic case (Fig. 11), giving rise to a shorter period spacing. We can also notice a more featured distribution of $\Delta\Pi$ vs Π for the Newtonian case, compared to the relativistic one. This is because in the Newtonian case, the propagation region (see the lower panel of Fig. 11) includes two bumps which are associated with the CO/He and He/H chemical transitions, while in the relativistic case, the bump associated with the CO/He interface is embedded in the solid core, where the modes cannot propagate, and thus it does not impact the mode-trapping properties of the model. Finally, we note that the kinetic energy values are globally higher for the relativistic model. This is due to the fact that this model is much more compact than its Newtonian counterpart, which implies macroscopic movements of the fluid in a much denser environment, and therefore, with greater kinetic energies.

5 SUMMARY AND CONCLUSIONS

We presented the first set of evolutionary sequences for CO UMWD models of 1.29, 1.31, 1.33, 1.35, 1.37, 1.38, and $1.382 M_{\odot}$, which fully take into account the effects of general relativity on their structural and evolutionary properties. These sequences extend the relativistic ONe UMWD sequences already computed in Althaus et al. (2022) to models with a CO-core composition. CO UMWDs can result either from single or binary stellar evolution. In this work, initial models for our evolving sequences were extracted from the full single evolution of an initially $7.8 M_{\odot}$ model that avoids C-ignition, and whose CO core slowly grows during the super asymptotic giant branch as a result of reduced wind rates (see Althaus et al. 2021). This progenitor evolution was computed with the Monash-Mount Stromlo code as presented in Gil-Pons et al. (2013, 2018). Calculations presented here were done with La Plata stellar evolution code, LPCODE, for which the standard stellar structure and evolution equations have been modified to include the effects of general relativity. For comparison purposes, additional sequences of identical initial models were computed for the Newtonian gravity case. Considering

that the number of UMWDs in the solar neighbourhood with mass determinations beyond about $1.30 M_{\odot}$ has substantially increased in recent years (e.g. Kilic et al. 2021), the calculations presented here are timely to study the properties of such stars. Also, from a sample of white dwarfs within 500 pc from the Sun, we identified a number of reasonable UMWD candidates with masses larger than $1.33 M_{\odot}$ for which general relativistic effects should be taken into account.

We provide mass-radius relations for relativistic CO UMWD sequences, cooling times, and magnitudes in *Gaia* DR3, Sloan Digital Sky Survey, and Pan-STARRS passbands using the non-grey model atmospheres of Koester (2010) and Koester & Kepler (2019). We find that CO white dwarfs more massive than $1.382 M_{\odot}$ become gravitationally unstable with respect to general relativity effects, being this limit higher than the limiting mass value of $1.369 M_{\odot}$ we found in Althaus et al. (2022) for ONe white dwarfs. As expected, the importance of general relativistic effects increases as the white dwarf mass increases. As the stellar mass approaches the limiting mass value, relative differences in radius (taking as a reference the relativistic model) reach up to 55%. Hence, for such massive white dwarfs, general relativity leads to white dwarf sequences that are markedly fainter than Newtonian sequences with the same mass. Therefore, the effects of general relativity effects must be carefully taken into account when determining the mass and stellar properties of such massive white dwarfs. We also find that the thermo-mechanical and evolutionary properties of the most massive white dwarfs are strongly affected by general relativity effects. As in the case of ONe white dwarfs studied in Althaus et al. (2022), we find that general relativity strongly alters the evolutionary properties of the most massive CO UMWDs, leading, at advanced stages of evolution, to much shorter cooling times than in the Newtonian case. We also find that for the most massive white dwarf models, the inclusion of general relativity effects lead to a gravitational redshift a factor 1.5 larger than predicted by the Newtonian white dwarf models (differences in the gravitational redshift are about 200 km s^{-1}).

The immediate prospect of detecting pulsating white dwarfs with masses above $\sim 1.30 M_{\odot}$ (see Kilic et al. 2023) motivated also us to assess in this work, for the first time, the impact of our new relativistic UMWD models on the pulsational properties of ultra-massive ZZ Ceti stars. To this end, we employed the LP-PUL pulsation code to perform an exploratory pulsational investigation by computing adiabatic g -mode Newtonian pulsations on fully relativistic equilibrium white dwarf models. We find that general relativity impacts the Brunt Väisälä frequency profile of the most massive models, substantially altering their g -mode pulsational properties such as the forward period spacing and the kinetic energy of oscillation.

Summarizing, general relativity effects should be taken into account for an accurate assessment of the structural, evolutionary, and pulsational properties of white dwarfs with masses above $\approx 1.30 M_{\odot}$. It should be appropriate to refer to such white dwarfs as *relativistic ultra-massive white dwarfs*. The relativistic CO ultra-massive white dwarf evolutionary sequences presented here constitute an improvement over those computed in the framework of Newtonian gravity. The impact of general relativity on the thermo-mechanical structure of the most massive white dwarfs could affect the energetics of the explosion and the nucleosynthesis of neutron-rich matter (and thus be relevant for the better understanding of type-Ia supernova explosions) as well as the critical density that separates the explosive and the collapse outcomes of these supernovae.

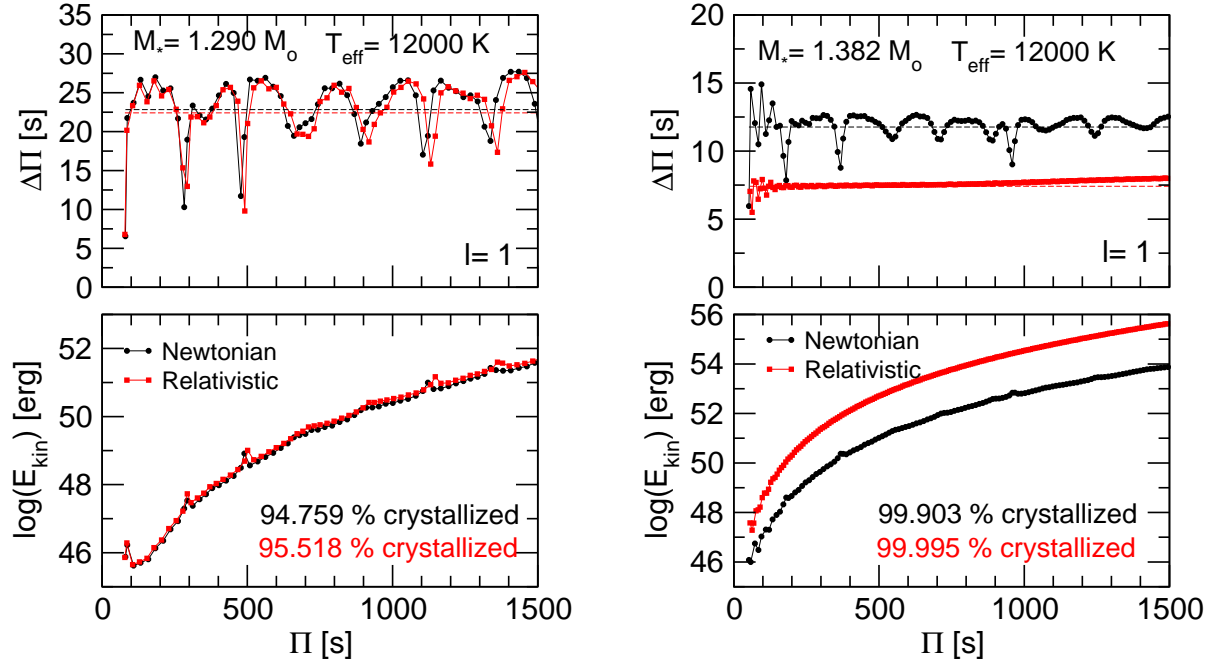


Figure 12. *Left panels:* the forward period spacing, $\Delta\Pi$ (upper panel), and the logarithm of the kinetic energy of oscillation, E_{kin} (lower panel), in terms of the pulsation periods, Π , corresponding to the template UMWD model with $M_* = 1.29 M_\odot$ and $T_{\text{eff}} \sim 12000 \text{ K}$ (see Fig. 10). The results corresponding to the Newtonian case are displayed using black curves and symbols, while the relativistic results are shown with red curves and symbols. *Right panels:* same as in the left panels, but for the template UMWD model with $M_* = 1.382 M_\odot$ and $T_{\text{eff}} \sim 12000 \text{ K}$ (Fig. 11).

ACKNOWLEDGEMENTS

We thank Domingo García-Senz for valuable comments about the possible impact of our models on Type Ia Supernovae and Detlev Koester for providing atmosphere models to the high surface gravities that characterise our relativistic ultra-massive white dwarf models. Part of this work was supported by PICT-2017-0884 from ANPCyT, PIP 112-200801-00940 grant from CONICET, and by the Spanish project PID 2019-109363GB-I00. MEC acknowledges Grant RYC2021-032721-I funded by MCIN/AEI/10.13039/501100011033 and by the European Union NextGenerationEU/PRTR. ST, RR and ARM acknowledge support from MINECO under the PID2020-117252GB-I00 grant and from the AGAUR/Generalitat de Catalunya grant SGR-386/2021. RR acknowledges support from Grant RYC2021-030837-I funded by MCIN/AEI/ 10.13039/501100011033 and by “European Union NextGenerationEU/PRTR”. This research has made use of NASA Astrophysics Data System. This work has made use of data from the European Space Agency (ESA) mission *Gaia* (<https://www.cosmos.esa.int/gaia>), processed by the *Gaia* Data Processing and Analysis Consortium (DPAC, <https://www.cosmos.esa.int/web/gaia/dpac/consortium>). Funding for the DPAC has been provided by national institutions, in particular the institutions participating in the *Gaia* Multilateral Agreement.

DATA AVAILABILITY STATEMENT

Supplementary material will be available to all readers. The cooling sequences are publicly available for download at <http://evolgroup.fcaglp.unlp.edu.ar/TRACKS/tracks.html>.

REFERENCES

- Althaus L. G., Serenelli A. M., Panei J. A., Córscico A. H., García-Berro E., Scóccola C. G., 2005, *A&A*, **435**, 631
- Althaus L. G., Córscico A. H., Isern J., García-Berro E., 2010, *A&ARv*, **18**, 471
- Althaus L. G., Camisassa M. E., Miller Bertolami M. M., Córscico A. H., García-Berro E., 2015, *A&A*, **576**, A9
- Althaus L. G., et al., 2021, *A&A*, **646**, A30
- Althaus L. G., Camisassa M. E., Torres S., Battich T., Córscico A. H., Rebassa-Mansergas A., Raddi R., 2022, *A&A*, **668**, A58
- Bergeron P., Kilic M., Blouin S., Bédard A., Leggett S. K., Brown W. R., 2022, *ApJ*, **934**, 36
- Bours M. C. P., et al., 2015, *MNRAS*, **450**, 3966
- Bravo E., García-Senz D., 1999, *MNRAS*, **307**, 984
- Caiazzo I., et al., 2021, *Nature*, **595**, 39
- Camisassa M. E., et al., 2019, *A&A*, **625**, A87
- Camisassa M. E., Althaus L. G., Koester D., Torres S., Pons P. G., Córscico A. H., 2022, *MNRAS*, **511**, 5198
- Carvalho G. A., Marinho R. M., Malheiro M., 2018, *General Relativity and Gravitation*, **50**, 38
- Chandra V., Hwang H.-C., Zakamska N. L., Cheng S., 2020, *ApJ*, **899**, 146
- Cheng S., Cummings J. D., Ménard B., Toonen S., 2020, *ApJ*, **891**, 160
- Christensen-Dalsgaard J., et al., 2020, *A&A*, **635**, A165
- Córscico A. H., Althaus L. G., 2006, *A&A*, **454**, 863
- Córscico A. H., Althaus L. G., Miller Bertolami M. M., Kepler S. O., 2019, *A&ARv*, **27**, 7
- Córscico A. H., Althaus L. G., Camisassa M. E., 2023, *arXiv e-prints*, p. [arXiv:2302.04100](https://arxiv.org/abs/2302.04100)
- Curd B., Gianninas A., Bell K. J., Kilic M., Romero A. D., Allende Prieto C., Winget D. E., Winget K. I., 2017, *MNRAS*, **468**, 239
- Dessert C., Long A. J., Safdi B. R., 2022, *Phys. Rev. Lett.*, **128**, 071102
- Doherty C. L., Gil-Pons P., Siess L., Lattanzio J. C., Lau H. H. B., 2015, *MNRAS*, **446**, 2599
- Doherty C. L., Gil-Pons P., Siess L., Lattanzio J. C., 2017, *Publ. Astron. Soc. Australia*, **34**, e056

- Dominguez I., Straniero O., Tornambe A., Isern J., 1996, *ApJ*, **472**, 783
- Fontaine G., Brassard P., 2008, *PASP*, **120**, 1043
- Gagné J., Fontaine G., Simon A., Faherty J. K., 2018, *ApJ*, **861**, L13
- García-Berro E., Ritossa C., Iben Icko J., 1997, *ApJ*, **485**, 765
- Gianninas A., Bergeron P., Ruiz M. T., 2011, *ApJ*, **743**, 138
- Gil-Pons P., Suda T., Fujimoto M. Y., García-Berro E., 2005, *A&A*, **433**, 1037
- Gil-Pons P., Doherty C. L., Lau H., Campbell S. W., Suda T., Guilani S., Gutiérrez J., Lattanzio J. C., 2013, *A&A*, **557**, A106
- Gil-Pons P., Doherty C. L., Gutiérrez J. L., Siess L., Campbell S. W., Lau H. B., Lattanzio J. C., 2018, *Publ. Astron. Soc. Australia*, **35**, 38
- Hermes J. J., Kepler S. O., Castanheira B. G., Gianninas A., Winget D. E., Montgomery M. H., Brown W. R., Harrold S. T., 2013, *ApJ*, **771**, L2
- Hollands M. A., et al., 2020, *Nature Astronomy*,
- Jiménez-Esteban F. M., Torres S., Rebassa-Mansergas A., Cruz P., Murillo-Ojeda R., Solano E., Rodrigo C., Camisassa M. E., 2023, *MNRAS*, **518**, 5106
- Kanaan A., Kepler S. O., Giovannini O., Diaz M., 1992, *ApJ*, **390**, L89
- Kepler S. O., et al., 2016, *MNRAS*, **455**, 3413
- Kilic M., Bergeron P., Blouin S., Bédard A., 2021, *MNRAS*, **503**, 5397
- Kilic M., Córscico A. H., Moss A. G., Jewett G., De Gerónimo F. C., Althaus L. G., 2023, *arXiv e-prints*, p. [arXiv:2304.10330](https://arxiv.org/abs/2304.10330)
- Kleinman S. J., et al., 2013, *ApJs*, **204**, 5
- Koester D., 2010, *Mem. Soc. Astron. Italiana*, **81**, 921
- Koester D., Kepler S. O., 2019, *A&A*, **628**, A102
- Mathew A., Nandy M. K., 2017, *Research in Astronomy and Astrophysics*, **17**, 061
- Miller Bertolami M. M., 2016, *A&A*, **588**, A25
- Montgomery M. H., Winget D. E., 1999, *ApJ*, **526**, 976
- Moriya T. J., 2019, *MNRAS*, **490**, 1166
- Mukadam A. S., et al., 2004, *ApJ*, **607**, 982
- Nitta A., et al., 2016, *IAU Focus Meeting*, **29**, 493
- Nunes S. P., Arbañil J. D. V., Malheiro M., 2021, *ApJ*, **921**, 138
- Pshirkov M. S., et al., 2020, *MNRAS*, **499**, L21
- Rauer H., et al., 2014, *Experimental Astronomy*, **38**, 249
- Ricker G. R., et al., 2014, in Oschmann Jacobus M. J., Clampin M., Fazio G. G., MacEwen H. A., eds, *Society of Photo-Optical Instrumentation Engineers (SPIE) Conference Series Vol. 9143, Space Telescopes and Instrumentation 2014: Optical, Infrared, and Millimeter Wave*. p. 914320 ([arXiv:1406.0151](https://arxiv.org/abs/1406.0151)), [doi:10.1117/12.2063489](https://doi.org/10.1117/12.2063489)
- Rotondo M., Rueda J. A., Ruffini R., Xue S.-S., 2011, *Phys. Rev. D*, **84**, 084007
- Rowan D. M., Tucker M. A., Shappee B. J., Hermes J. J., 2019, *MNRAS*, **486**, 4574
- Salaris M., Althaus L. G., García-Berro E., 2013, *A&A*, **555**, A96
- Scholz R.-D., 2022, *Research Notes of the American Astronomical Society*, **6**, 36
- Schwab J., 2021a, *ApJ*, **906**, 53
- Schwab J., 2021b, *ApJ*, **916**, 119
- Siess L., 2006, *A&A*, **448**, 717
- Siess L., 2010, *A&A*, **512**, A10
- Silva Aguirre V., et al., 2020, *A&A*, **635**, A164
- Temmink K. D., Toonen S., Zapartas E., Justham S., Gänsicke B. T., 2020, *A&A*, **636**, A31
- Thorne K. S., 1977, *ApJ*, **212**, 825
- Torres S., Canals P., Jiménez-Esteban F. M., Rebassa-Mansergas A., Solano E., 2022, *MNRAS*, **511**, 5462
- Ventura P., D'Antona F., 2011, *MNRAS*, **410**, 2760
- Wang B., Liu D., Chen H., 2022, *MNRAS*, **510**, 6011
- Winget D. E., Kepler S. O., 2008, *ARA&A*, **46**, 157
- Wu C., Xiong H., Wang X., 2022, *MNRAS*, **512**, 2972

This paper has been typeset from a $\text{\TeX}/\text{\LaTeX}$ file prepared by the author.